

Uniaxial tension– Compression behaviour of the UHPFRC using GGBS

Tensão uniaxial– Comportamento em compressão do UHPFRC usando GGBS

Rosangel Rojas Agüero^{1*}, Jose Rafael Yopez Aguirre¹, Christa Korzenowski², Ronaldo Beraldin³

ABSTRACT

The purpose of this study was to investigate the mechanical characteristics of Ultra-High Performance Fibre Reinforced Concrete (UHPFRC) under compression uniaxial loading conditions, using waste in the mixture. UHPFRC is a class of cementitious material with high durability and strength, limited to a minimum value of compressive strength of 150 MPa. The difference with traditional concrete lies mainly in the post-peak behaviour that occurs due to the presence of fibres, which are responsible for ensuring the ductile behaviour of the material. Uniaxial compression tests on twenty cylindrical specimens were carried out and tested after 28 days of curing, with a percentage of steel fibres of 1% at a displacement loading speed of 0.5 mm/min. The mixture design that was used allowed to manufacture a thixotropic material, characterized by a compressive strength and an average modulus of elasticity of 150.89 MPa and 47.71 GPa respectively. A simple production process was used, including Ground Granulated Blast Furnace Slag (GGBS) as the main sustainable material and as partial substitute for cement. Curves for design and structural analysis were plotted and compared with the average experimental curve and with other research consulted in the literature, including the elastic and inelastic behaviour of the material.

Keywords: UHPFRC; GGBS; Compression behaviour; Modulus of elasticity; Post peak.

RESUMO

O objetivo deste trabalho foi investigar as características mecânicas do Concreto de Ultra-Alto Desempenho Reforçado com Fibras (CUADRF) sob condições de carregamento uniaxial de compressão, utilizando resíduos na mistura. CUADRF é uma classe de material cimentício com alta durabilidade e resistência, limitada a um valor mínimo de resistência à compressão de 150 MPa. A diferença com o concreto tradicional está principalmente no comportamento pós-pico que ocorre devido à presença de fibras, responsáveis por garantir o comportamento dúctil do material. Ensaios de compressão uniaxial em vinte corpos de prova cilíndricos foram realizados e testados após 28 dias de cura, com uma porcentagem de fibras de aço de 1% a uma velocidade de carregamento por deslocamento de 0,5 mm/min. A dosagem da mistura utilizada permitiu a fabricação de um material tixotrópico, caracterizado por uma resistência à compressão e um módulo de elasticidade médio de 150,89 MPa e 47,71 GPa, respectivamente. Foi utilizado um processo de produção simples, incluindo a Escória de Alto Forno Granulada (EAFG) moída como principal material sustentável e substituto parcial do cimento. As curvas para o dimensionamento e análise estrutural foram traçadas e comparadas com a curva experimental média e com outras pesquisas consultadas na literatura, incluindo o comportamento elástico e inelástico do material.

Palavras-chave: CUADRF; EAFG; Comportamento em compressão. Módulo de elasticidade. Pós-pico.

¹Universidade Federal de Rio Grande. *E-mail: r.rojas@furg.br

²Universidade Estadual de Rio Grande do Sul.

³Universidade Federal de Rio Grande do Sul.

INTRODUCTION

Ultra-High-Performance Fibres Reinforced Concrete (UHPFRC) is a class of cementitious material with high strength, ductility in both compression and traction, and great durability, which is limited to a minimum compressive strength (f_c) of 150 MPa, (ACI 233R, 1995 and AFGC, 2013).

Some authors, such as Walraven (2012) recommend, as an optimal solution to ensure competitiveness in various UHPFRC applications, to manufacture mixtures to achieve a f_c of 130 MPa. López (2017) refers to the French standard that proposes a minimum characteristic compressive strength (f_{ck}) of 130 MPa obtained from cylindrical specimens of 150 mm diameter and 300 mm height, or 145 MPa for 100 mm cubic specimens.

Schmidt and Fehling (2005) point out four principles that must be met to achieve ultra-high strength and durability in concrete: (i) a very low water/cement ratio of approximately 0.20 to 0.25, which results in a very dense and strong structure, minimizing pore capillarity and preventing the transport of toxic gases and liquids into and through the concrete; (ii) high particle packing, especially for fine aggregate, reducing the water demand for fresh concrete, increasing f_c and also increasing the brittleness of the concrete; (iii) the use of a large amount of superplasticizer, to adjust workability; (iv) the use of fibres to increase tensile strength, flexural strength, and shear resistance and to make the concrete sufficiently ductile.

The superior qualities mentioned in the previous paragraph make UHPFRC a suitable solution for structures where high strength and durability properties are required. Since its first appearance, this material has been used in numerous structural applications in the field of bridges, pavements and architectural structures, Behlou et al. (2013).

Great engineering works are being built in the main countries of the world with UHPFRC, examples of which can be consulted in the ACI 233R (2018) report. Research must be carried out considering the conditions and local resources available in Latin American countries, with the premise of establishing structural design standards and building, in the near future, engineering constructions using this novel material.

The components of the material include steel fibres, cement, mineral additives, silica sand (SS), superplasticizer and water, to form a dense matrix without coarse aggregate with low porosity and high strength. Among the mineral additives, Ground

Granulated Blast Furnace Slag (GGBS) is added as the main sustainable component in the mixture.

Sustainable development has become a global goal of the construction industry, achieving ultra-high strength using industrial waste is a real challenge. The high material cost, high energy consumption and CO₂ emissions of the UHPFRC are the typical disadvantages that restrict its wider application.

Efforts to obtain energy savings must be consolidated. To reduce the economic and environmental disadvantages, the approaches are in most cases limited to the applications of industrial by products or waste materials without sacrificing the materials mechanical performance, as we do in this research.

This research was part of a series of studies carried out as support to an invention patent. It was deposited with the National Institute of Industrial Property (INPI) of Brazil, with registration number BR102020024167 (ROJAS et al., 2020). The purpose was to investigate the mechanical characteristics of Ultra-High Fibres Reinforced Concrete (UHPFRC) under compression uniaxial loading conditions, using wastes in the mixture.

THEORETICAL BASES OF RESEARCH

To reflect the behaviour of concrete by means of stress-strain diagrams (σ - ϵ) is a widely used method, mainly to relate compressive strength to modulus of elasticity (E_c). However, the σ - ϵ response of concrete to compression can exhibit significant variation because, among other things, concrete is a heterogeneous material with no standardized mix designs.

Considering an important feature from these constitutive relationships for the UHPFRC, as is the linearity of behaviour in the ascending branch, we can calculate the value of E_c in a range of stresses outside significant nonlinearity. This nonlinearity occurs because concrete begins to develop internal micro-cracks and therefore exhibit reduced stiffness as compressive stresses increase.

Another way to calculate the modulus of elasticity is by numerical equations relating E_c to f_c . In the ACI 318R (2005) we can find one of the simplest and most widely used relationships between f_c and E_c for concrete, where these two variables are related through a linear multiplier, see Eq. 1. Other more sophisticated relationships may include a term for density, high compressive strength at different fractional powers or the inclusion of a constant term, as was formulated by Neville (1995) and Popovics (1973).

$$E_c = 4730 \sqrt{f_c}; (f_c \text{ in MPa}) \quad (1)$$

Graybeal (2005) indicated two equations that more closely predict the results observed in his UHPFRC studies, Equation (2) from the proposed ACI 363R (1992) for concretes up to 83 MPa and Equation (3) from Ma et al. (2004) derived from the UHPFRC experimental results without coarse aggregates.

$$E_c = 3320 \sqrt{f_c} + 6900; (f_c \text{ in MPa}) \quad (2)$$

$$E_c = 19000 \sqrt[3]{\frac{f_c}{10}}; (f_c \text{ in MPa}) \quad (3)$$

Yoo et al. (2016) used ASTM C469 to calculate the modulus of elasticity. Each compression test is described by an σ - ϵ curve, and then E_c can be calculated from it by the following expression:

$$E_c = \frac{0,4 \cdot f_c - f_1}{\epsilon_2 - 0,00005}; (f_c, f_1 \text{ in MPa}) \quad (4)$$

Where:

f_c : Ultimate compressive strength

f_1 : Stress corresponding to the strain of 0.00005

ϵ_2 : Strain produced by stress in 40% of f_c

Alsaman et al. (2017) carried out an extensive investigation of the experimental data published in the literature to propose an expression that predicts the value of the modulus of elasticity as a function of the f_c of the UHPFRC, see Eq. 5.

$$E_c = 8,010 (f_c)^{0,36}; (f_c \text{ in MPa}) \quad (5)$$

Several authors have determined the compressive strength and modulus of elasticity of UHPFRC using procedures similar to those reflected in this paper, some of which are briefly described below.

Graybeal (2008) reached 179.95 MPa of maximum compressive strength, without registering post-peak behavior and calculated the modulus of elasticity using a linear approximation with better adjustment in the results of the curve σ - ϵ from 10% to 30% of the compressive strength, reaching 52 GPa. It is important to highlight some aspects of his experimental work: (i) the author used dry materials premixed by a commercial company, which provided large quantities of material from the same batch with al-most

identical quality assurance and properties in each delivery; (ii) he included 2% steel fibers; (iii) in addition to the water-reducing additive, a setting accelerator was used, which allows to accelerate the strength gain at early ages.

The same author, in Graybeal (2005), recommends using the behavior curves to determine the modulus of elasticity in the range of 5% and 80% of the peak or maximum compressive strength for heat-treated specimens on cure and 5% to 70% of f_c for non-heat-treated specimens, with eight weeks of curing and using 2% steel fibers.

Mahmud et al. (2013) used 2% steel fibers and the heat treatment applied included a higher curing temperature. They achieved 151 MPa and 45 GPa for compressive strength and modulus of elasticity respectively.

Shafieifar et al. (2017) worked with 2% steel fibers and included additional ground quartz and a mixture setting accelerator. The premixed dry materials were supplied by a commercial company, with quality assurance, who delivered for the researchers ready for the experimental work. No heat treatment was applied during curing. The maximum compressive strength and modulus of elasticity values were 138 MPa and 60 GPa. The authors calculated the modulus of elasticity using a linear approximation with a best fit in the range of 10% to 30% of the peak compressive strength.

Singh et al. (2017) tested the specimens at the age of 56 days, at a displacement loading rate of 0.05 mm/min, i.e., 10 times less than that used in the present work. The percentage of steel fibres added to the mixture was 2.25%. The values of maximum compressive strength and modulus of elasticity were 143 MPa and 38 GPa respectively.

Krah et al. (2018) fabricated the test bodies using 1% steel fibers in the mixture. The cylinders were tested at a displacement loading speed of 0.005 mm/s, i.e. 40% less than that used in this study. The specimens were stored in a wet chamber for 28 days and then subjected to a thermal curing treatment, which consisted of submerging them in water for seven days at 70°C. The values of f_c and E_c were 142.13 MPa and 38.69 GPa respectively. The authors calculated the modulus of elasticity at 40% of the ultimate load.

Osta et al. (2017) manufactured the specimens using 2% steel fibers of two types in the mixture: (i) 50% short and straight fiber; (ii) 50% long fiber with a hook at the ends. The maximum compressive strength and modulus of elasticity values were 128 MPa and 46 GPa respectively. The authors did not apply heat treatment on curing.

In the present study, we will characterize the compression behaviour of UHPFRC

following the AFGC (2013) guidelines. An experimental program will be developed and the graphic response of each test will be recorded to determine mechanical parameters of the material, following guidelines obtained from the bibliographic review.

EXPERIMENTAL PROGRAM

A practical strategy widely used in experimental programs to analyze the results of concrete resistance tests is the factorial arrangement, in which different treatments that are to be compared are defined. In the design of treatments, controllable factors, their levels and the combination between them are selected. The experimental design indicates the way in which the treatments are randomized and the way to control their natural variability.

The statistical tools indicated in the previous paragraph were used to define the UHPFRC mixture design used in this study, whose development can be consulted in more detail in Rojas et al. (2019). These publications explain the extensive experimental work carried out, the end result of which is the design of the mixture indicated in Table 1, which allows the production of UHPFRC with a compressive strength greater than 150 MPa.

Table 1 – UHPFRC mix design.

Material	kg/m ³
Cement	955
GGBS	263
Silica Fume	119
Quartz powder	119
Fine sand	788
Superplasticizer	40
Water	185

Source: Authors, 2019.

The experimental work developed in the present study differs from those carried out in Rojas et al. (2019) by determining post-peak compression behaviour. Registering the inelastic phase of UHPFRC in uniaxial compression is not an easy task, mainly because after the first crack appears, LVDTs lose vertical stability and cannot adequately measure the deformation in the inelastic phase.

To record the inelastic phase of the behaviour, the methodology proposed by Hassan et al. (2012) is applied, for which a total of twenty cylindrical specimens are fabricated and tested at a speed of 0.5 mm/min, which is the minimum speed of the machine available in the laboratory. The behaviour curves are plotted and the modulus of elasticity is determined by linear approximation in the elastic phase of the material.

Materials

The agglomerating materials used in the mixture are made up of:

- National cement type Portland CP V ARI with high initial resistance.
- Ground Granulated Blast Furnace Slag (GGBS) donated by the company ArcelorMittal Tubarão in the Brazilian state of Espírito Santo. In Table 2 we observe the chemical composition of the GGBS used in this research, including the ranges recommended in ACI 233R (1985).
- Commercial silica fume (SF).
- Commercial quartz powder.

It has a single aggregate consisting of silica sand with a maximum grain size of 0,30 mm. A solution of polycarboxylate in an aqueous medium (Visco-Crete 3535) supplied by SIKA was used as a super-plasticizer additive, which adjusts the workability of the concrete and is mixed with normal water to be placed in the mix.

Table 2 – Chemical composition of GGBS.

Main chemical constituents	Percent by mass	Range ACI 233R
CaO	44.50%	32-45%
SiO ₂	30.22%	32-42%
Al ₂ O ₃	7.92%	7-16%
Fe ₂ O ₃	7.45%	0.1-1.5%
MnO	1.10%	0.2-1.0%
MgO	1.08%	5-15%

Source: Authors, 2019.

The fiber used is of the steel Dramix type, 13 mm long and 0.2 mm in diameter, in a volume equal to 1%. Table 1 shows the proportions of the mixture, in which 26% of the cement is replaced by sustainable materials (GGBS and SF) and 8% is replaced by quartz powder. The water/cement ratio is 0.19 and the water/binder ratio is 0.13.

The AFGC (2013) recommends using cylindrical specimens to determine the compressive behavior of UHPFRC, specifying diameters that depend on the length of the fiber to be used, in order to avoid agglomerations of material within the shape that can create voids and influence the strength of the concrete matrix.

For fibers of 13 mm in length, it is recommended to use forms with 11 cm in diameter and 22 cm in height, however, the machine available in the laboratory does not have the capacity to failure test bodies with ultra-high resistance and with those dimensions. Therefore, the experimental work is adapted to the resources available in the laboratory.

Manufacturing the Mixture

The UHPFRC mixture developed in this research has a simple manufacturing process, without the need for elaborated and delayed grinding processes for the packaging of particles. Two types of industrial waste are included in the mixture, silica fume and mainly GGBS, the latter with a specific granulometric distribution indicated in the invention patent.

The materials are weighed and placed in a mixer in the following order: silica fume, cement, and blast furnace slag and silica sand. The dry materials are mixed for about 5 minutes before the superplasticizer previously mixed with the water is added to the mixture. Wet materials are mixed for about 10 minutes.

Initially, a dry mix is observed until small spheres of material are formed; about 1 mm in diameter, these spheres get mixed together and progressively increase in diameter until they become a wet concrete paste, see Figure 1.

Figure 1 – Formation of spheres in the mixture.



Source: Authors, 2019.

It is observed how the material separates from the bottom of the mixer, acquiring the shape and consistency of a dense plastic mass, see Figure 2. In this state, the mixture for the UHPFRC is considered ready and it is in this moment that the steel fibers are placed, mixing for approximately 2 minutes.

Figure 2 – Mixture consistency.



Source: Authors, 2019.

After fabrication, the mixture is cast into the respective moulds, to be compacted on a vibrating table for 1 minute. The specimens are stored and covered with a plastic layer for 48 hours, after which they are placed in a thermal bathroom for 24 hours at a temperature of 60 °C and then at 90 °C for another 24 hours. They are then stored in a humid room at 23 ± 3 °C until the day of the test, avoiding in all cases thermal shock on the specimens.

Uniaxial compression test

From an experimental point of view, the compilation of consistent and accurate stress vs. strain data (σ - ϵ) is difficult. This is mainly due to the increasingly nonlinear behaviors that concrete tends to exhibit as the maximum strength value is reached and exceeded. Even if the downward branch of the behavior is ignored as compressive strength is reached, the observed stress behavior of the concrete is highly dependent on the experimental loading and stress measurement techniques employed.

During the execution of the compression test, when the first crack forms, the lateral deformation exceeds its tensile capacity and the UHPRC specimens (without fibers) lose their total strength and fail in an abrupt and explosive manner. In contrast, UHPFRC specimens (with fibers) behave elastically up to approximately 80 to 90 % of their compressive strength. After reaching the maximum resistance (f_c), a progressive strain softening takes place in which the presence of fibers regulates the softening stage in a similar way as it happens in tensile, to later produce the ductile compression failure.

In the standards NBR 7215 (1996) and NBR 5739 (2007) the guidelines to perform the compression test on cylindrical specimens are specified. Standards BS 1881-121 (1983) and ASTM C469-94 (1994) specify the procedure to obtain the elasticity module and the σ - ϵ behavior in compression.

Hassan et al. (2012) found that the latter two methods are not appropriate for measuring post-peak behavior of UHPFRC. In the first case, according to BS, it is possible to determine the static modulus of elasticity, but the test is not capable of capturing post-peak behavior, because when cracking begins the gauges detach from the specimen and give erroneous results. In the second case, according to ASTM, two rigid circular rings are used, which are secured at approximately two-thirds of the height of the specimen using clamping pins, and two LVDTs are used inserted between the rings. However, when the shear failure occurs the clamping pins turn and measure erroneously.

For the reasons mentioned above the author proposes a third measurement method, which consists of placing the circular rings with the LVDTs in the specimen only to measure the elastic state of the test. Additionally, two LVDTs are placed parallel to the specimen to measure the movement of the test machine head, allowing the recording of the post-peak stage. In the linear elastic part, the author calculates the value of the strain by dividing the average displacements of the LVDTs by the initial length of measurement maintained by the circular rings. Later, with the appearance of the first crack, a multiple cracking phase occurs, in which the strain is obtained by dividing the average displacement of the external LVDTs (those that measure the displacement of the machine head) by the total height of the specimen. The stress in this stage was obtained by dividing the machine load by the cross-sectional area of the cylinder.

METHOD

The method explained in the previous paragraph was used in this research with the purpose of recording the post-peak behavior of the UHPFRC subjected to uniaxial compression. The twenty specimens, with 28 days of cure, were tested, applying monotonic displacement loading, using a 2000kN hydraulic machine at a rate of 0.5 mm/min, see Figure 3. The uniaxial compression test was performed on specimens manufactured using steel molds of 50 mm diameter by 100 mm height, containing a 1% fiber volume and following the criteria specified in the ABNT NBR7215 (1996) standard. Previously, the superior and inferior face of each cylinder was leveled mechanically using a rectifier and its height is measured to verify the necessity of applying some correction factor in the resistance according to item 6.1.2 Table 2 of ABNT NBR5739 (2007).

Figure 3 – Post-peak measurement in uniaxial compression test.



Source: Authors, 2019.

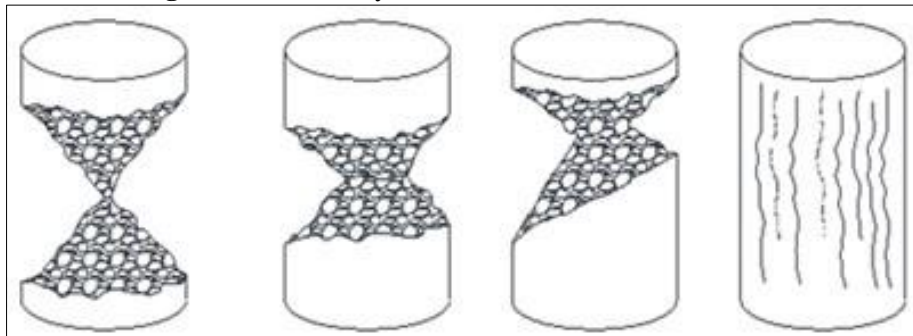
The values of the load vs. vertical displacement of each specimen are recorded, to later calculate the resistance values obtained by dividing the load applied by the cross-sectional area of the cylinder. The vertical elastic displacement was measured by LVDTs on the cylinder until the first crack appeared and the inelastic was measured by LVDT located between the lower and upper face of the machine head in contact with the test body, see Figure 3.

Characteristic compressive strength

To determine the characteristic compressive strength (f_{ck}) of the UHPFRC, the AFGC (2013) recommendations are used, indicating the procedure to be followed:

1. Apply the displacement control load.
2. The fracture surface must be consistent with Figure 4, specified in EN: 12390 (2001), which indicates the types of satisfactory failure that must occur in cylindrical specimens.
3. The average strength must be calculated on at least three specimens.
4. The characteristic compressive strength value is calculated by subtracting the Student's coefficient multiplied by the standard deviation from the average strength value.

Figure 4 – Boundary element and element SOLID 185.



Source: Authors, 2019.

Modulus of elasticity

The modulus of elasticity was calculated by measuring directly on the linear upward branch of the UHPFRC constituent curve, recorded for each of the uniaxial compression tests performed on cylindrical specimens. A linear approximation is used with best fit σ - ϵ results between 0 and 80 % of the peak compression strength. The value of E_{cm} is then defined as the average modulus of elasticity of the UHPFRC or the average

secant modulus of elasticity, calculated as the average of the twenty individual values obtained graphically.

Compressive behaviour for design purposes

Considering the experimental data, the AFGC (2013) recommends, for regulatory calculations in the ultimate limit state at flexure, a conventional linear constitutive law in compression with a yield plateau. Following the specifications of chapter 2 item 2.2 of that standard, we can plot an analytical curve for the UHPFRC's law of behavior in compression for structural design, as specified below.

The recommendations indicate that the beginning of the yield plateau corresponds to the maximum stress (f_{cd}) equal to $0.85 f_{ck} / \gamma$, where γ is equivalent to the partial safety coefficient for concrete, given by EN1992-1-1 (2004) equal to 1.5. The strain ϵ_{cd} corresponds to the stress f_{cd} and can be calculated as the quotient between f_{cd} and E_{cm} . The strain ϵ_{cud} is equivalent to a more complex expression given by:

$$\epsilon_{cud} = \epsilon_{cd} \left[1 + 14 \frac{f_{ctfm}}{f_{cm}} \right]; \quad (f_{ctfm}, f_{cm} \text{ in MPa}) \quad (6)$$

The f_{ctfm} value corresponds to the maximum average post-cracking tensile stress, which will be taken from Rojas (2019) located in item 7.2.1. The value of f_{cm} corresponds to the maximum average stress at compression, whose value will be determined in this paper. With these simple calculations, an analytical behavior curve for UHPFRC design can be established.

Post-Peak Compression Constitutive Behaviour

The Annex 2 Part B of the AFGC (2013) recommendations establishes a procedure for determining the compression behavior curve for UHPFR including the post-peak phase. The procedure is semi-analytical, applied when only certain experimental parameters such as maximum compressive strength (f_{cm}), modulus of elasticity (E_{cm}) and maximum tensile strength (f_{ctfm}) are known, as explained below.

The first step is to determine the deformation $\epsilon_{1,f}$ corresponding to f_{cm} . Considering the confinement effect provided by the fibers, we can use Equations 7 and 8. The k_0 factor is the ratio of E_{cm} (MPa) to the cubic root of f_{cm} (MPa).

$$\epsilon_{1,f} = \left[1 + 4 \frac{f_{ctfm}}{f_{cm}} \right] \epsilon_{c1}; \quad (f_{ctfm}, f_{cm} \text{ in MPa}) \quad (7)$$

$$\varepsilon_{c1} = \left[1 + 0,16 \frac{k_0}{f_{cm}^2 + 800} \right] \frac{f_{cm}^{2/3}}{k_0}; \quad (f_{cm} \text{ in MPa}) \quad (8)$$

The strain ε_{c2} that corresponds to 70 % of f_{cm} is calculated using Equations 9 and 10. For all cases f_{cm} is expressed in MPa.

$$\varepsilon_{c2, f} = \left[1 + 15 \frac{f_{ct} f_m}{f_{cm}} \right] \varepsilon_{c2}; \quad (f_{ct} f_m, f_{cm} \text{ in MPa}) \quad (9)$$

$$\varepsilon_{c2} = \left[1 + \frac{20}{f_{cm}} \right] \varepsilon_{c1}; \quad (f_{cm} \text{ in MPa}) \quad (10)$$

The analytical compression behavior law can be obtained using the Popovics curve. If $x = \varepsilon / \varepsilon_{c1, f}$; $y = \sigma / f_{cm}$; $X = \varepsilon_{c2, f} / \varepsilon_{c1, f}$; the law is as follows:

$$y = \frac{n \cdot x}{n - 1 + x^{\varphi \cdot n}}; \quad (f_{cm} \text{ in MPa}) \quad (11)$$

Where: $n = k / (k - 1)$; $k = E_{cm} \cdot \varepsilon_{c1, f} / f_{cm}$; $\varphi = 1$ on the branch ascending; and $\varphi = \ln(1 - n + n \cdot X) / (n \cdot \ln X)$ on the branch descending to obtain $y = 0,7$ in $x = X$.

RESULTS AND DISCUSSIONS

Uniaxial compression tests were carried out by applying displacement load, and the failure pattern presented in the specimens tested can be seen in Figure 5. Specimens that showed failure patterns different from those specified in the English standard were discarded.

Figure 5 – Type of failure in specimens made with UHPFRC.



Source: Authors, 2019.

Cylinders containing 2% of fibers were tested, in all cases the results showed resistance values significantly lower than those manufactured with 1% of fibers and therefore were discarded. We presumed that reduction of strength was due to fiber agglomerations and the formation of internal voids.

Table 3 shows the results obtained for specimens containing 1% of fibers. For each test and for the average curve the behavior curve σ - ϵ was obtained, see Figure 6, and the value of maximum compressive strength was recorded. From each behavior curve (σ - ϵ) the value of the modulus of elasticity was obtained. It was measured in the elastic phase, considering a linear approximation with best fit in the results from 0% to 80% of f_c .

Table 3 – UHPFRC compressive strength and modulus of elasticity (1MPa=145psi).

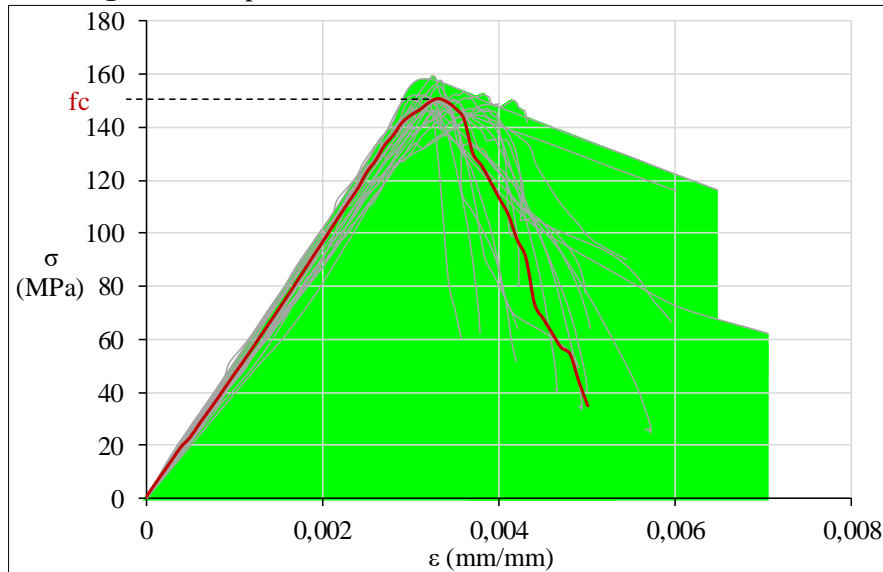
Specimen	σ (MPa)	E (MPa)
1	154	50709
2	147	44504
3	146	46104
4	158	49551
5	150	48209
6	150	46780
7	146	47503
8	152	45802
9	153	44548
10	155	46556
11	144	43768
12	159	50799
13	147	47035
14	150	49184
15	150	49129
16	150	48193
17	146	45522
18	150	49293
19	152	49595
20	158	51374
Average:	151	47708

Source: Authors, 2019.

The average values of both compressive strength (f_{cm}) and the modulus of elasticity (E_{cm}) are shown in the last line of the Table 3, which gave values of 150.89 MPa and 47.71 GPa with standard deviation of 4.32 and 2.24 GPa respectively. The strain corresponding to f_{cm} was 0.00331. The characteristic resistance value (f_{ck}) was 143.43 MPa with a 95% probability of exceedance, obtained using the Student-fisher law.

The description in the previous paragraph meets the recommendations of the AFGC (2013), which propose to characterize the compression behavior of UHPFRC according to the values of the characteristic compression strength and the modulus of elasticity. Table 4 compares characteristic resistance values (f_{ck}) of different mix designs consulted in the literature with that achieved in the present study. From that analysis we can indicate the following aspects:

Figure 6 – Experimental constitutive behavior of the UHPFRC.



Source: Authors, 2019.

1. In most cases ultra-high strength is achieved by the application of particle packing to densify the concrete matrix, with the exception of references Habel et al. (2006), Rossi et al. (2005), Lim and Nawy (2005) and Kahanji (2017) which do not indicate the use of this technique in their procedures.
2. Kahanji et al. (2017) worked with the same percentage of fiber used in this research, with additional similarities in the type of mixing and blending. These authors achieved a strength 7.22% higher than ours, possibly due to the type of curing used, which consisted in immersing the specimens in water for seven days at 90 °C, accelerating the gain in strength to a greater extent at early ages.
3. Most of the references use fiber quantities higher than 1%. High fiber contents can represent significant increases in the total cost of UHPFRC; Camacho (2013) reports increase between 60-80% for fiber percentages between 1.5-2.5%. Furthermore, if the fiber content is exceeded, the rheology is affected by the agglomeration of fibers in the mixture with the consequent decrease in strength. In our case, a decrease in resistance was observed in the laboratory when testing cylinders with 2% of fibers. Those specimens presented resistances between 100-120 MPa; for this reason, they were excluded from the present research.
4. The water/cement (w/c) and water/binder (w/b) ratios in our research are among the lowest. These values follow the basic principle indicated by Camacho (2013) to obtain ultra-high resistance to compression. The author

indicates that the water not used by the cement in the hydration process should be as little as possible, so that capillary porosity and its connections are minimal, increasing resistance and durability. The author also makes another recommendation, attended by all the references in the table, referring to the type of additives used in the manufacture of UHPFRC, which can reduce the water content by up to 40%; these are the plasticizers based on polycarboxylate, which belong to the so-called third generation.

5. As in the present study, Hassan et al. (2012), Yang et al. (2009), Thanh (2008), Wu et al. (2016) and Lampropoulos et al. (2016) were able to decrease the amount of cement and increase the compressive strength with the use of GGBS together with silica fume (SF). The use of these two industrial wastes allows for the densification of the matrix, the reduction of the heterogeneity of the concrete and makes it possible to add a high volume of fibers to the mix, if the ductility of the material is to be increased. They also help control the speed and amount of hydration heat in the concrete and thus reduce thermal stress, i.e., can prevent thermal cracking of the concrete.

Table 4 – Mix design comparison for UHPFRC.

Reference	Cement	GGBS	SF	Quartz	Sand	w/b	w/c	Fibres %	fck MPa
	kg/m ³								
Hassan, 2012	657	418	119	0	1051	0.15	0.28	2	151
Yu, 2014	875	0	43.7	0	1273	0.22	0.23	2.5	149
Habel, 2006	1050	0	275	0	730	0.14	0.18	6	168
Yang, 2009	657	430	119	0	1050	0.15	0.28	2	190
Larrad, 1994	1081	0	334	0	813	0.14	0.18	0	238
Rossi, 2005	1050	0	268	0	514	0.16	0.20	5	205
Lim, 2005	543	0	80	0	1242	0.21	0.24	1.5	121
Graybeal, 2007	710	0	230	210	1020	0.14	0.15	2	193
Thanh, 2008	657	418	119	0	1051	0.15	0.28	2.5	186
Toledo ¹ , 2012	1011	0	58	0	962	0.17	0.16	2	162
Wu, 2016	863	315	216	0	1079	0.18	0.21	2	-
Lamprop., 2016	657	418	119	0	1051	0.15	0.28	3	164
Hoang, 2017	795	0	169	198	971	0.16	0.24	1.5	212
Kahanji, 2017	967	0	251	0	675	0.20	0.25	1	155
Rojas, 2019	955	263	119	119	788	0.13	0.19	1	143

¹ It uses 76 kg/m³ Wollastonite microfibers

Source: Authors, 2019.

The aspects indicated above, which define the mix design used in the current document, allowed the mechanical properties that characterize ultra-high-performance concretes to be achieved. In addition, it was possible for the material to exhibit thixotropic behavior, see Figure 7, a characteristic that opens up a range of application possibilities,

for example for structural reinforcement, where architectural flexibility, time and type of placement govern the viability of the project.

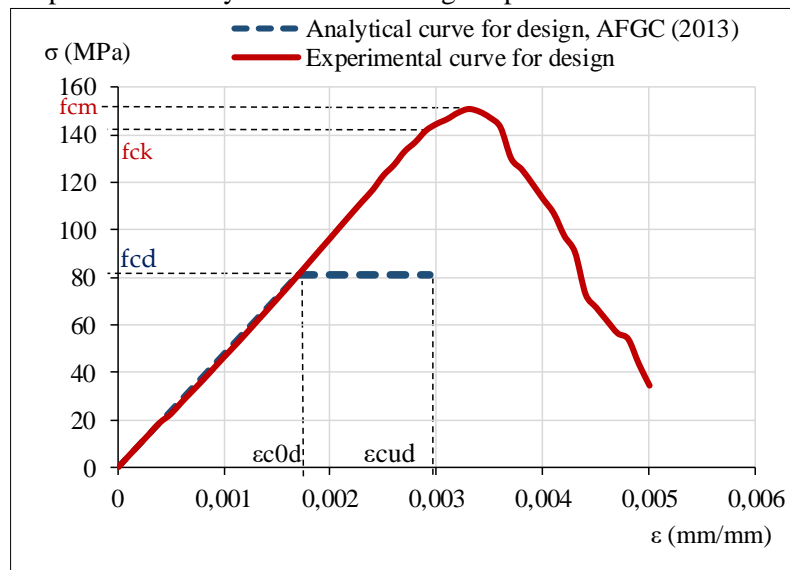
The Figure 8 shows the graph of the UHPFRC behavior curve for the structural design, constructed following the recommendations of the AFGC (2013), and it is compared with the average experimental curve of our study. The f_{cd} , f_{ctfm} and ϵ_{c0d} values were 81.28 MPa; 7.78 MPa; 0.0017 respectively. These data are substituted in Equation 6 and a value of 0.0029 is obtained for ϵ_{cud} .

Figure 7 – Thixotropic of the UHPFRC mixture.



Source: Authors, 2019.

Figure 8 – Comparison of analytical versus average experimental behavior for the UHPFRC.



Source: Authors, 2019.

The French standard recommends using the safety factor of 1.50 indicated by the English standard for UHPFRC, which reduces the compressive strength of the material by 33% in relation to the characteristic strength. We also note that the value of the ultimate design strain is 12% lower than the strain corresponding to f_{cm} . So, it is possible to think that the ductility of the material after the ultimate strain is reached can be considered as a

safety remnant. In the following, each phase of the compression behavior is analyzed individually.

Linear elastic behaviour, phase I

Observing the elastic phase plotted in the Figures 7 to 12, we notice a practically linear behaviour until almost reaching the maximum resistance of the matrix, showing that there is no evident damage at that stage. The strain corresponding to the maximum average stress was 0.33% for UHPFRC, with a difference of more than 50% compared to the same strain in traditional concrete, which is usually 0.2%.

The average modulus of elasticity, measured in the ascending phase of the behaviour curve, is compared in Table 5 with the analytical or experimental results obtained by other authors consulted in the literature, from which we can indicate the following aspects:

1. The modulus of elasticity varies in the range of 38 and 60 GPa and the value reached in this study is within that range.
2. Similarities in stiffness are observed, except when the formula recommended by ACI 318R (2005) is used, which reflects an overestimation in the value of E_c and in Shafieifar et al. (2017) and get a 26% higher value. In the latter case the authors used a premixed, industrialized mixture produced and sold by an American company with high quality standards, which decreases the experimental variability. They also included ground quartz, which improves the quality of the mixture.
3. However, the average behaviour curve resulting from this study is almost identical to the results of Graybeal (2005); Mahmud et al. (2013); Krahl et al. (2018) and Osta et al. (2017) see Figure 12; when we compare the values of E_c for each author included in Table 5, we can observe that for the last three cases there are differences, i.e. there should be both numerical and graphical similarity. It was found that this difference is due to the selection of the range within the curve to measure E_c . In some cases, the modulus of elasticity was measured in a linear approximation very close to the origin (between 0 - 10% of f_{cm}), and in others in an intermediate range (between 30 - 40% of f_{cm}).
4. With the exception of Krahl et al. (2018) all the references indicated in Table 5 worked with mixtures containing 2% of fibre, that is, twice the amount considered

in this work. We noted then that this difference in the quantity of fibres did not have a significant influence on the calculation of the modulus of elasticity.

Table 5 – Elastic module, comparison with various authors.

Author	Ecm (MPa)	Variance (%)
ACI-318R (2018)	58102	+21.79
Graybeal B. (2005)	47169	-1.13
ACI-363R (1992)	47682	-0.05
Ma et al. (2004)	469502	-1.59
Als Salman et al. (2017)	48747	+2.18
Mahmud et al. (2013)	45000	-5.68
Shafieifar et al. (2017)	60000	+25.77
Singh et al. (2017)	38000	-20.35
Krahl et al. (2018)	39000	-18.25
Osta et al. (2017)	46000	-3.58
Rojas R. et al.	47708	

Source: Authors, 2019.

Inelastic behaviour, phase II

The post-peak behavior was recorded in 55% of the sample, of the twenty tests performed, only in eleven of the cases it was possible to record the inelastic behavior. The results of the remaining nine specimens were discarded because they presented measurements not compatible with the elastic phase.

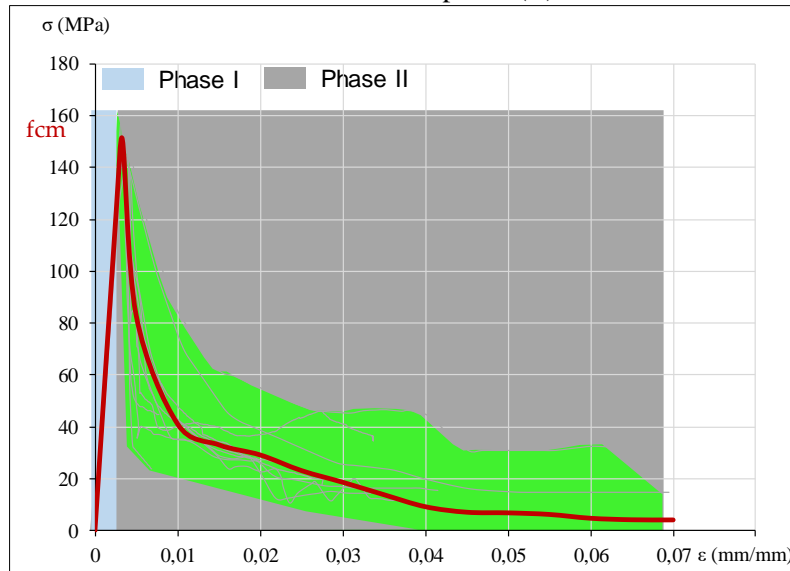
It is important to note that the measurement procedure used is sensitive to any instability produced by external agents, such as drops in electrical voltage or defects in the connectors of the instruments, which may affect the measurement during the performance of the experiment.

In this phase, permanent strain and multiple micro-cracks occur, the curves obtained present a concave shape with a constant decrease in resistance after the maximum effort is reached, which indicates that the UHPFRC can support a certain load capacity through large strain without reaching the fragile failure.

In Figure 9 each experimental test was plotted, including the average curve, with its phase I elastic and phase II inelastic. We noticed that after reaching the maximum resistance, the curves present a loss of rigidity, multiple micro cracking on the cylinders become visible and graphically a progressive strain softening is observed. In this state, the presence of the fibers governs the behavior, similar to what happens in traction. A change of slope in the curves is observed between the range of 30 and 60 MPa, the strain

increases rapidly and the load is maintained with little variation, until the test is completed. In all cases the elements showed ductile compression failure.

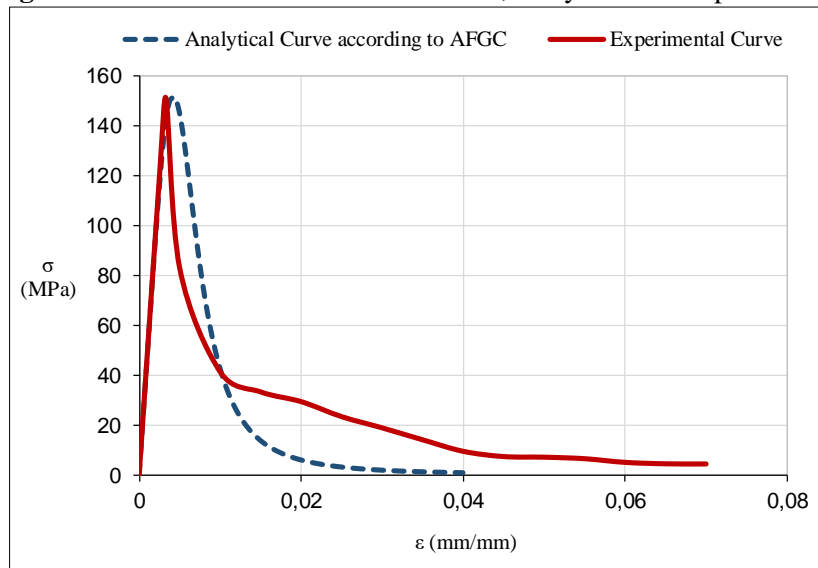
Figure 9 – Constitutive experimental behavior of the UHPFRC indicating the elastic phase (I) and the inelastic phase (II).



Source: Authors, 2019.

Figure 10 compares graphically the compression behavior of the average experimental UHPFRC with the analytical curve calculated according to the specifications of the AFGC (2013), following the procedure indicated in item 3.4 and using Equation 11.

Figure 10 – Law behavior of the UHPFRC, analytical and experimental.



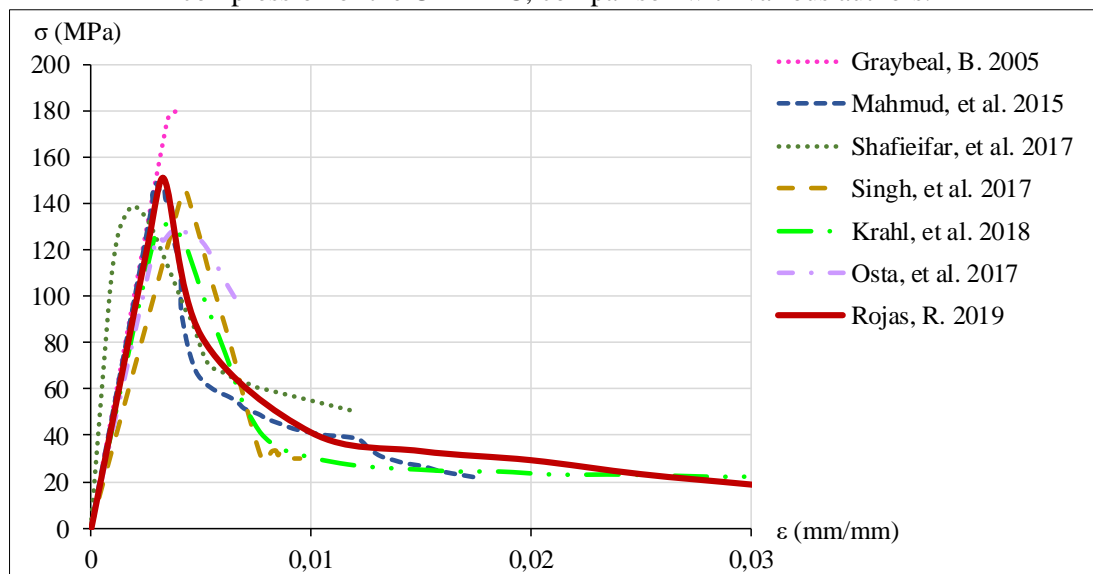
Source: Authors, 2019.

The experimental ductility was 21% higher than analytical ductility, considering 0.04 as the value for the ultimate strain. We have that the value of the experimental

ductility was 12.08 with value of 0.00331 for the yield strain, and, the value of the analytical ductility was 9.98 with value of 0.00401 for the yield strain. When compared with the post-peak analytical response, the experimental curve underestimates the behavior in the descending branch, and then overestimates it in the large strain branch, where the load decrease between 40 and 10 MPa.

Figure 11 compares the average UHPFRC experimental curve obtained in this study with the results of several researchers cited in the literature. For the inelastic phase there are similarities with Mahmud et al. (2013), Singh et al. (2017) and Krahl et al. (2018). In the inelastic phase, where the fibers govern behavior, the average curve of this study is higher than some of the references that use higher fiber contents. It is assumed that this overestimation of the results is caused by performing the experiments at a significantly higher loading speed than those used in the references cited.

Figure 11 – Law behavior of the UHPFRC, analytical and experimental constitutive behavior in compression of the UHPFRC, comparison with various authors.



Source: Authors, 2019.

CONCLUSIONS

The UHPFRC was characterized by its behavior in uniaxial compression, relating elastically and inelastically stresses and strains. From these relationships, values above 150 MPa and 48 GPa were obtained for compressive strength and modulus of elasticity respectively. The mix design proposed in this research to reach these values takes into account the following characteristics: (i) water/cement ratio of 0.19; (ii) water/binder ratio

of 0.13; (iii) inclusion of 1% of short steel fibers; (iv) use of industrial waste as a partial substitute for cement.

The post-peak behavior was recorded in 55% of the sample using a simple measurement method. Nine specimens were discarded because they presented measurements not compatible with the elastic phase. The measurement procedure used was very sensitive to any instability produced by external agents, such as drops in electrical voltage or difficulty in correctly leveling the LVDTs fixed on the machine with the supports available in the laboratory, which affected the record during the performance of the experiment.

The average experimental curve of the UHPFRC reflected 21% higher ductility than the average analytical curve. Post-peak behavior was overestimated when compared to other experimental results and the average analytical curve, possibly caused by conducting the experiments at a significantly higher rate than that used in the reference literature.

There is no clear consensus to define the elastic linear range over which the value of the modulus of elasticity can be graphically determined. The differences presented depend on the selection of the range within the curve and not on the fiber percentage.

Most of the specimens continued to bear the load after reaching the design value of the ultimate strain, decreasing in a smooth manner to a load of approximately 5 MPa, after which it remains almost constant.

This behavior admits the possibility of reducing the values of the safety factor when using UHPFRC, considering that experimentally a great ductility is reflected graphically after the last design strain is reached, and when comparing the value of the safety coefficient of 1.5 used for UHPFRC with that of 1.4 recommended for conventional concrete, that presents a type of fragile failure.

ACKNOWLEDGMENTS

This research was supported by the Programa de Pós-graduação em Engenharia Civil PPGEC-UFRGS and was funded by the Coordenação de Aperfeiçoamento de Pessoal de Nível Superior (CAPES) do Ministério de Educação of Brazil. Also like to show our gratitude to the company AcerlorMittal Tubarão and SIKA-Brazil for the donation of material for the research.

REFERENCES

- ALSALMAN, A.; DANG, C.; PRINZ, G. AND HALE, M. Evaluation of modulus of elasticity of ultra-high performance concrete. **Construction and Building Materials Journal**. v. 153, p. 918-928, 2017.
- AMERICAN CONCRETE INSTITUTE. **ACI 233R-95**: Ground granulate blast-furnace slag cementitious constituent in concrete. ACI, 1995.
- AMERICAN CONCRETE INSTITUTE. **ACI 239R-18**: Ultra-High-Performance Concrete: An Emerging Technology Report. ACI, 2018. ISBN 978-1-64195-034-3
- AMERICAN CONCRETE INSTITUTE. **ACI 318R-05**: Building code requirements for structural concrete and commentary. ACI, 2005.
- AMERICAN CONCRETE INSTITUTE. **ACI 363R-92**: Guide to Quality Control and Testing of High-Strength Concrete. ACI, 1992.
- AMERICAN SOCIETY FOR TESTING AND MATERIALS. **ASTM C469**: Standard Test Method for Static Modulus of Elasticity and Poisson's Ratio of Concrete in Compression. ASTM, 1994.
- ASSOCIAÇÃO BRASILEIRA DE NORMAS TÉCNICAS. **ABNT NBR 5739**: Concreto. Ensaio de compressão de corpos de prova cilíndricos. Rio de Janeiro: ABNT, 2007.
- ASSOCIAÇÃO BRASILEIRA DE NORMAS TÉCNICAS. **ABNT NBR 7215**: Cimento Portland Determinação da Resistência à Compressão. Rio de Janeiro: ABNT, 1996.
- ASSOCIATION FRANÇAISE DE GÉNIE CIVIL. **AFGC**: Ultra-High-Performance Fiber Reinforced Concretes. Recommendations. AFGC, 2013.
- Behloul M, Batoz J. Ductal applications over the last Olympiad. In: **Proceedings international symposium on ultra-high performance concrete**, pp. 855-862, Kassel, Germany, 2013. ISBN 978-3-89958-376-2.
- CAMACHO, Esteban Torregrosa. **Dosage optimization and bolted connections for UHPFRC ties**. 2013. Thesis (Doctor of Sciences UPV) - Universitat Politècnica de València, Valencia, Spain, 2013.
- EUROPEAN STANDARD. **EN: 12390-3**: Testing hardened concrete - Part 3: Compressive strength of test specimens. EN, 2001.
- EUROPEAN STANDARD. **EN 1992-1-1**: European Standard. Design of concrete structures - Part 1-1: General rules and rules for buildings. European Standard. EN, 2004.
- EUROPEAN STANDARD. **EN: BS 1881-121**: Static modulus of elasticity in compression. BS, 1983.
- GRAYBEAL BENJAMIN. **Characterization of the behavior of Ultra High-Performance Reinforced Concrete**. 2005. PhD Thesis. University of Maryland, USA.
- GRAYBEAL, B. Compressive behavior of Ultra-High Performance Fiber Reinforced Concrete. **Journal ACI Materials**, v. 104, n. 2, p. 146-152, 2007.
- GRAYBEAL B. UHPC in the **US Highway Transportation System**. In: **INTERNATIONAL SYMPOSIUM ON ULTRA HIGH PERFORMANCE CONCRETE**, Kassel, Germany, p. 11-18, 2008. ISBN 978-3-89958-376-2
- HABEL, K.; VIVIANI, M.; DENARIÉ, E.; BRÜHWILER, E. Development of the mechanical properties of an Ultra-High Performance Fiber Reinforced Concrete

- (UHPC). **Cement and Concrete Research Journal**, v. 36, p. 1362-1370, 2006.
- HASSAN, A.; JONES, S.; MAHMUD, G. Experimental test methods to determine the uniaxial tensile and compressive behavior of ultra-high performance fiber reinforced concrete (UHPC). **Journal Construction and Building Materials**, v. 37, p. 874-882, 2012.
- HOANG, A. and FEHLING, E. Influence of steel fiber content and aspect ratio on the uniaxial tensile and compressive behavior of ultra-high-performance concrete. **Construction and Building Materials Journal**, v. 153, p. 790-806, 2017.
- KAHANJI, Ch.; ALI, F.; NADJAI, A. Structural performance of ultra-high performance fiber-reinforced concrete beams. **Journal Structural Concrete**, v. 18, p. 249-258, 2017.
- KRAHL, P.; SALEME, G.; AND CARRAZEDO, R. Compressive behavior of UHPC under quasi-static and seismic strain rates considering the effect of fiber content. **Construction and Building Materials Journal**, v. 188, p. 633-644, 2018.
- LAMPROPOULOS, A.; PASCHALIS, S.; TSILOULOU, O.; DRITSOS, S. Strengthening of reinforced concrete beams using ultra high performance fiber reinforced concrete (UHPC). **Journal Engineering Structures**, v. 16, p. 370-384, 2016.
- LARRARD, F. and SEDRAN, T. Optimization of Ultra-High-Performance Concrete by the use of a packing model. **Cement and Concrete Research Journal**, v. 24, n. 1, p. 997-1009, 1994.
- LIM, D.H. and NAWY, E. G. Behavior of plain and steel-fiber-reinforced high-strength concrete under uniaxial and biaxial compression. **Journal Magazine of Concrete Research**, v. 57, n. 10, p. 603-610, 2005.
- LOPEZ Juan Angel. **Characterization of the tensile behavior of UHPC by means of four-point bending test**. 2017. PhD These. University Polytechnic of Valencia, Spain, 2017.
- MA, J.; ORGASS, M.; DEHN, F.; SCHMIDT, D. Comparative investigation on ultra-high-performance concrete with and without coarse aggregate. In: **Proceeding International Symposium on Ultra High-Performance Concrete (UHPC)**, Kassel, Germania, 2004. ISBN 978-3-89958-086-0.
- MAHMUD, G.; YANG, Z.; AND HASSAN, A. Experimental and numerical studies of size effects of Ultra High Performance Steel Fiber Reinforced Concrete (UHPC) beams. **Construction and Building Materials Journal**, v. 48, p. 1027-1034, 2013.
- NEVILLE, A. **Properties of Concrete**. 4th ed. Addison Wesley Longman Limited, Wigtown, United Kingdom, pp. 844, 1995.
- OSTA, M.; ISA, M.; BALUCH, AND RAHMAN, M. Flexural behavior of reinforced concrete beams strengthened with ultra-high performance fiber reinforced concrete. **Construction and Building Materials Journal**, v. 134, p. 279-296, 2017.
- POPOVICS, S. A numerical approach to the complete stress-strain curve of concrete. **Journal Cement and Concrete Research**, v. 3, n. 5, p. 583-599, 1973.
- ROJAS, Rosangel Agüero. **Estudio experimental y numérico de vigas usando Ultra-High Performance Reinforced Concrete-UHPC**. 2019. Tesis (Doutorado em Engenharia Civil área de Estruturas) – Universidade Federal de Rio Grande do Sul, Porto Alegre, Brazil, 2019.
- ROJAS R.; KORZENOWSKI C.; YEPEZ J.; BERARDIN R.; CAMPOS A.; MAGHOUS S. **Composição de concreto, processo de obtenção de uma composição de concreto e usos de uma composição de concreto**. Depositante: Universidade

Federal do Rio Grande do Sul. Depósito: BR102020024167. Protocolo: 870200017039. Instituto Nacional de Propriedade Industrial (INPI), Janeiro 2020.

ROJAS, R.; KORZENOWSKI, C.; YÉPEZ, J.; BERARDIN, R.; CAMPOS, A.; PINTO L. Investigando diseños de mezcla para producir ultra high performance fiber reinforced concrete (UHPRFC) usando ANOVA. **Revista Matéria**, UFRJ, v. 24, n. 2, 2019.

ROJAS, R.; KORZENOWSKI, C.; YÉPEZ, J.; CAMPOS, A.; PINTO, L.; MALLMANN, C. Estudio experimental de mezclas de concreto para producir UHPRC usando materiales brasileños sustentables. **Structures and Materials Journal**. Revista RIEM-IBRACON, v. 12, n. 4, 2019.

ROSSI, P.; ARCA, A.; PARANT, E.; FAKHRI, P. Bending and compressive behaviors of a new cement composite. **Cement and Concrete Research Journal**, v.3 5, n. 1, p. 27-33, 2005.

Schmidt, M.; Fehling, E. Ultra-High-Performance Concrete: Research, Development and Application in Europe. **International Concrete Abstracts Portal**, v. 228, p. 51-78. January 2005.

SHAFIEIFAR, M.; FARZAD, M.; AND AZIZINAMINI, A. Experimental and numerical studies on mechanical properties of Ultra High Performance Concrete (UHPC). **Construction and Building Materials Journal**, v. 156, p. 402-411, 2017.

SINGH, M.; SHEIKH, A.; ALI, M. VISINTIN, P. AND GRIFFITH, M. Experimental and numerical studies of the flexural behavior of ultra-high performance fiber reinforced concrete beams. **Construction and Building Materials Journal**, v. 138, p. 12-25, 2017.

THANH, LE, **Ultra high performance fiber reinforced concrete paving flags**. 2008. Ph. D Thesis, University of Liverpool, Liverpool, U.K.

TOLEDO, R.; KOENDERS, E.; FORMAGINI, S.; FAIRBAIRN, E. Performance assessment of Ultra High Performance Fiber Reinforced Cementitious Composites in view of sustainability. **Journal Materials and Design**, v.3 6, p. 880-888, 2012.

WALRAVEN, J. On the way to international design recommendations for Ultra High Performance Fiber Reinforced Concrete. In: **Proceedings of the International Symposium on UHPC and Nanotechnology for High Performance Construction Materials**, pp. 51-58, Kassel, Germany, 2012. ISBN 978-3-86219-265-6.

WU, Z.; SHI, C.; KHAYAT, K. Influence of silica fume content on microstructure development and bond to steel fiber in ultra-high strength cement based materials (UHSC). **Journal Cement and Concrete Composites**, v. 71, p. 97-109, 2016.

YANG, S.L.; MILLARD, S.G.; SOUTSOS, M.N.; BARNETT, S.J.; LE, T.T. Influence of aggregate and curing regime on the mechanical properties of ultra-high performance fiber reinforced concrete (UHPRFC). **Journal Construction and Building Materials**, v. 26, n. 6, p. 2291-2298, 2009.

YU, R.; SPIESZ, P.; BROUWERS, H. Mix design and properties assessment of Ultra High-Performance Fiber Reinforced Concrete (UHPRFC). **Cement and Concrete Research Journal**, v. 56, p. 29-39, 2014.

YOO, D.; BANTHIA, N.; YOON, Y. Predicting service deflection of ultra-high performance fiber reinforced concrete beams reinforced with GFRP bars. **Materials Composites Journal**. Part B, v. 99, p. 381-397, 2016.

Recebido em: 20/05/2022

Aprovado em: 25/06/2022

Publicado em: 29/06/2022